Surface structure of anatase $TiO_2(001)$: Reconstruction, atomic steps, and domains

Yong Liang,* Shupan Gan, and Scott A. Chambers
Environmental Molecular Sciences Laboratory, Pacific Northwest National Laboratory, Richland, Washington 99352

Eric I. Altman
Department of Chemical Engineering, Yale University, New Haven, Connecticut 06520
(Received 21 December 2000; published 10 May 2001)

The surface structure of anatase $TiO_2(001)$ was investigated using scanning tunneling microscopy (STM), x-ray photoelectron spectroscopy (XPS), reflection high-energy electron diffraction (RHEED), and low-energy electron diffraction (LEED). A two-domain $(1\times4)/(4\times1)$ reconstruction, similar to those previously reported in LEED and ion scattering studies, was observed by STM and RHEED. This reconstruction was found to be stable not only from room temperature to 850 °C in ultrahigh vacuum and oxygen-rich environments, but also during the anatase film growth. High-resolution STM images obtained at positive sample biases revealed two types of atomic row within each surface unit cell, indicating different Ti-derived states at the surface. At the same time, XPS of the reconstructed surfaces showed no evidence of Ti^{3+}. Based on the STM, XPS, RHEED, and LEED results, an ''added''-and-''missing''-row model is proposed to account for the (1×4) reconstruction. Atomic steps and their relationship to the population of (1×4) and (4×1) domains were also investigated. The results showed that for vicinal surfaces the domain population depended strongly on the overall surface step orientation. While populations of the (1×4) and the (4×1) domains were nearly equal on flat (001) surfaces, they became significantly lopsided on a surface with its normal 2° away from the (001) direction, demonstrating a strong correlation between surface steps and domain population on vicinal surfaces.

DOI: 10.1103/PhysRevB.63.235402 PACS number(s): 68.35.Bs, 81.05.Je, 68.37.Ef, 75.70.Kw

I. INTRODUCTION

Titanium dioxide is of great importance in several technological applications including photocatalysis, sensors, solar cells, and memory devices.[1–4] TiO_2 has three different polymorphs: rutile, anatase, and brookite. The bulk and surface properties of rutile have received the most investigation due largely to the availability of large bulk rutile single crystals. Although anatase TiO_2 exhibits superior photocatalytic properties as well as a number of interesting behaviors,[4–8] experimental investigations on anatase single-crystal surfaces have been very limited and existing results remain controversial. Durinck *et al.* first reported a (1×1) low-energy electron diffraction (LEED) pattern from a mineral anatase (001) surface.[9] Recently, Herman, Sievers, and Gao reported a (1×4) reconstruction on thin-film anatase $TiO_2(001)$ surface.[10] Based on angle-resolved mass spectroscopy of recoiled ions, these authors attributed the (1×4) reconstruction to microfaceting toward (103) and $(\bar{1}03)$ surface planes. Hengerer *et al.* also reported a (1×4) reconstruction on anatase (001) surfaces. They suggested that this reconstruction might be due to ordered oxygen vacancies,[11] but they also cautioned about potential complications of this reconstruction. In this paper, we report on a study of the anatase $TiO_2(001)$-(1×4) surface by scanning tunneling microscopy (STM), combined with x-ray photoelectron spectroscopy (XPS), reflection high-energy electron diffraction (RHEED), and LEED. The nature of the reconstruction is explained in terms of ''added'' and ''missing'' rows at the anatase surfaces.

After a brief description of the experimental method, we present the RHEED, LEED, and STM results on the (1×4) reconstruction at the anatase $TiO_2(001)$ surface under different conditions. We then show XPS results on the electronic structures of $TiO_2(001)$-(1×4). We present evidence for atomic steps, defects on anatase (001) surfaces, and discuss the implications of these features for the surface reconstructions and domain populations. We finally propose a structural model that accounts for the surface reconstruction and local step structures.

II. EXPERIMENTAL METHOD

The experiments were conducted in two separate UHV systems. The first one is a custom-designed oxygen-plasma-assisted molecular-beam epitaxy (OPA-MBE) system that consists of a growth chamber and a characterization chamber. The growth chamber is equipped with a RHEED system operating at 15 keV for *in situ* monitoring of surface structure and morphology during film growth, an electron cyclotron resonance (ECR) plasma source for activated oxygen radicals, and two quartz crystal oscillators (QCO's) adjacent to the substrate for flux monitoring. The characterization chamber is equipped with an x-ray photoelectron spectrometer and reverse-view LEED optics. The second UHV system is equipped with a STM, LEED optics, an XPS spectrometer, an Auger electron spectrometer and an ECR oxygen plasma source. All the STM images shown here were taken at positive sample bias. The base pressures of both characterization chambers were in the low 10^{-10} Torr range. In both systems, sample heating was accomplished through electron bombardment from the back side of the sample holder, and the sample temperature was measured by a type-*K* thermocouple located adjacent to the sample. The detailed descriptions of these two systems have been provided elsewhere.[12,13]

Two classes of single-crystal anatase $TiO_2(001)$ surfaces were examined. The first class consisted of single-crystal anatase TiO_2 thin films. These films were grown on Nb-doped $SrTiO_3(001)$ substrates using the OPA-MBE method with the substrates at 550 °C and an oxygen pressure of 2×10^{-5} Torr. The film growth rate was typically ~1 Å/min, judged by the QCO's. The combination of low growth temperature and low growth rate was important in this case as it allowed the strontium out-diffusion from the $SrTiO_3$ substrates to the anatase films to be minimized while maintaining a high degree of crystallinity of the films. Upon completion of MBE growth, anatase films were transferred *in situ* to the appended characterization chamber for XPS and LEED measurements, and then transferred to the STM system through air for further investigations. After the *ex situ* sample transfer, the anatase films were subjected to several cycles of Ar sputtering and annealing in oxygen at a partial pressure of $\sim5\times10^{-8}$ Torr. XPS showed that the resulting surfaces were free of carbon contamination. However, cycles of sputtering and annealing often yielded a small amount of Sr residing at the anatase surfaces due to strontium segregation from the $SrTiO_3$ substrates. The amount of Sr was approximately 1 to 1.5 at. % based on XPS measurements. The quality of the LEED patterns of the resulting surfaces was either comparable to or better than that of as-grown anatase surfaces. In addition to LEED and RHEED, x-ray diffraction (XRD) was also used to verify the crystal structure of the MBE-grown anatase films. Results showed that these films consisted of 100% anatase and had no detectable minority phases.

The second class of single-crystal anatase was a bulk mineral. The sample surface was prepared by first annealing in an oxygen plasma at about 500 °C to remove all the Ca and carbon impurities at the surface and then in UHV at ~700 °C for several hours. The resulting surface exhibited sharp LEED patterns, comparable to those of the thin-film surfaces. Since the size of the mineral anatase sample was much smaller than the viewing area of the XPS spectrometer, Auger electron spectroscopy was used to verify the cleanliness of the surface. Results obtained after these treatments showed that the surface was free from Ca, Sr, and C impurities.

III. RESULTS

A. Surface reconstruction

Anatase TiO_2 has a tetragonal unit cell within which each Ti atom is coordinated to six oxygen atoms. Figure 1 shows a ball-and-stick model of an anatase unit cell. It contains 12 atoms and has a volume of $3.78\times3.78\times9.51$ Å^3. Compared to rutile TiO_2, there is a significant degree of buckling associated with O-Ti-O bonds in anatase. This buckling reduces the crystal symmetry and results in a larger unit-cell dimension in the [001] direction. Also notice in Fig. 1 that near the top of the unit cell the rows of oxygen atoms along [010] buckle upward, while $\frac{1}{2}$ a unit cell down, the rows of oxygen atoms along [100] buckle upward; this 90° rotation of the buckling direction is dictated by the crystal structure. There are two possible terminations for a (001) anatase surface. A

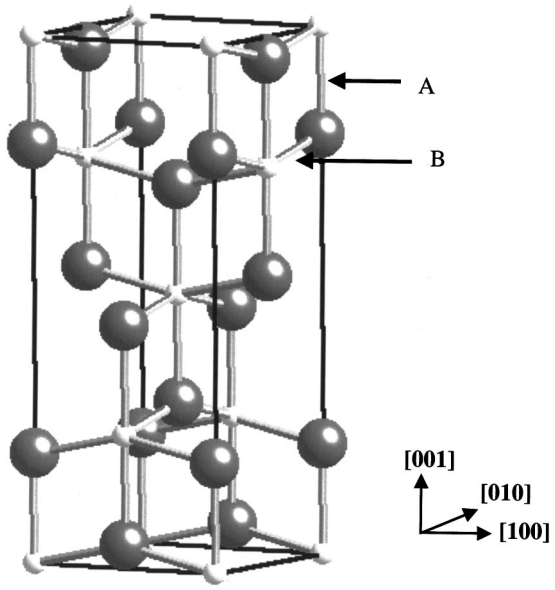

FIG. 1. A ball-and-stick model of an anatase unit cell. The large and small balls represent O and Ti atoms, respectively. The *A* and *B* markers denote different locations where the crystal may be cleaved.

(001) surface can be created either by breaking all the Ti-O bonds running along the [001] direction at the location marked *A* in Fig. 1, or by breaking not only the Ti-O bonds running along the [001] direction, but also those buckled O-Ti-O bonds at location *B*. The former creates an autocompensated surface; the latter not only involves more bond breaking events, but also yields a charged and thus energetically unstable surface terminated by Ti.

Figure 2(a) shows a RHEED pattern of an anatase surface taken along the [100] azimuthal direction during film growth. The streakiness of the pattern suggests that the film surface was very flat. Aside from the primary $1\times$ diffraction pattern, weak $4\times$ diffraction features consisting of three additional streaks within each $1\times$ structure were also visible, suggesting that a $4\times$ reconstruction occurred along the [010] direction during growth. Likewise, the RHEED patterns taken along the [010] azimuth also exhibited similar features, indicating either that the $4\times$ reconstruction was due to a mutually orthogonal two-domain surface structure, or that the reconstruction occurred along both [100] and [010] directions.

To elucidate the nature of the $4\times$ reconstruction observed by RHEED along both [100] and [010] directions, LEED was used to examine the anatase $TiO_2(001)$ surface. Figure 2(b) shows a LEED pattern for an as-grown anatase (001) surface. A two-domain structure, consisting of (1×4) and (4×1) reconstructions, similar to those reported by Herman *et al.* and by Hengerer *et al.*,[10,11] is clearly evident. A similar LEED pattern was also observed on the mineral $TiO_2(001)$ surface that was free of Sr, indicating that the (4×1) reconstruction is intrinsic to the anatase (001) surface, instead of due to Sr impurities or potential complications from the thin films such as stress due to the 3.5% lattice mismatch between the TiO_2 film and $SrTiO_3$ substrate.

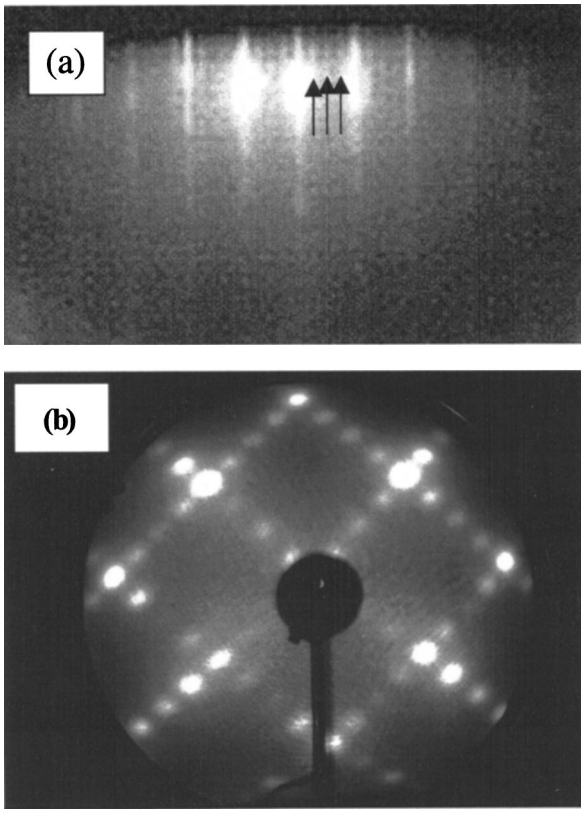

FIG. 2. (a) A RHEED pattern obtained during anatase film growth. In addition to the 1× diffraction features, a weak 4× diffraction pattern consisting of three additional lines (marked by three arrows) within the 1× pattern is also visible. (b) A LEED pattern of an as-grown TiO_2(001) surface showing a two-domain (1×4)/(4×1) reconstruction.

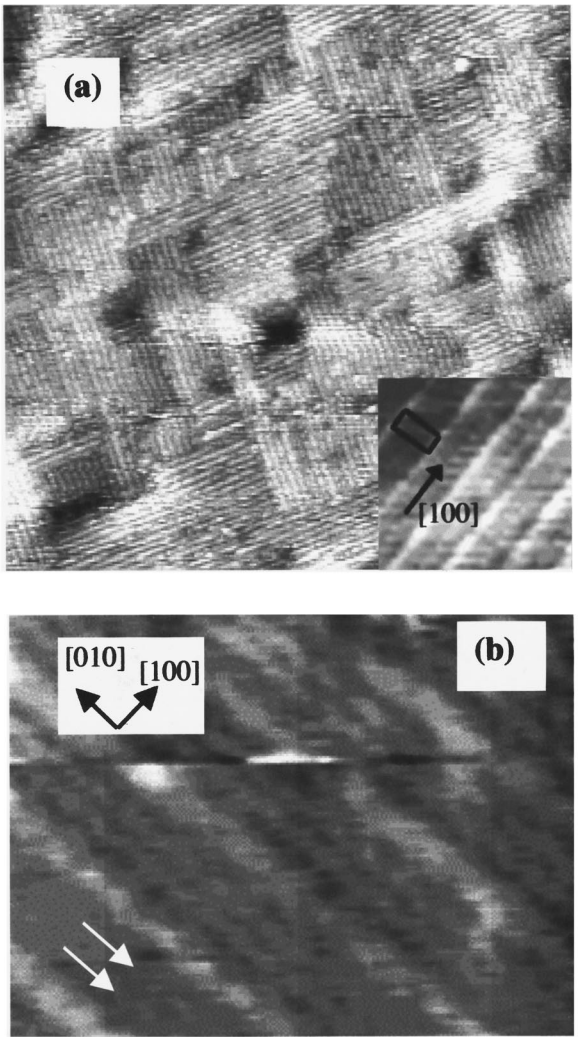

FIG. 3. (a) A large-scale STM image showing (1×4) and (4×1) domains on anatase TiO_2(001). The size of the image is 1200×1200 Å^2. The inset is a close-up view of the surface showing a (1×4) unit cell on TiO_2(001). (b) A high-resolution STM image reveals in addition to the bright rows two additional faint rows (marked by arrows) in each 4× period. (c) A magnified STM image showing a local 3× reconstruction on an anatase TiO_2(001) surface. The image is 170×40 Å^2 in size.

To better understand this reconstruction, we used STM to investigate the atomic structure and morphology of anatase TiO_2(001). Figure 3(a) is a large-scale STM image of an anatase film surface. Two types of mutually orthogonal domains separated by steps are shown in the image. The height of these steps was approximately 2.3 Å. Within experimental error, these steps corresponded to $\frac{1}{4}$-unit-cell-high atomic steps of 2.4 Å. There were essentially two types of step on this surface, with step edges either parallel or perpendicular to the atomic rows at the upper terraces. The former often had straight edges, while the latter typically had a high kink density, and were thus more kinky and wavy in appearance, similar to the *A* and *B* steps on Si(001) surfaces.[14] As on the Si surface, this suggests that steps running parallel to the atomic rows are lower in energy.

The average spacing between two adjacent atomic rows was ~16 Å, approximately four times the (1×1) unit cell distance (15.12 Å). In addition to the 4× periodicity, corrugations along the atomic rows with periodicity of ~4 and 8 Å, such as those shown in the inset of Fig. 3(a), were also observed. It is worth noting that the (1×4) and (4×1) domains shown in Fig. 3(a) are crystallographically equivalent. As shown in Fig. 1, a ''lower'' terrace can be reproduced from an upper terrace by a single-height vertical translation (2.4 Å), accompanied by a 90° rotation along the [001] axis, and followed by a 1.9 Å horizontal translation.

Figure 3(b) is a high resolution STM image of TiO_2(001)-(1×4). In addition to the brighter rows such as those shown in Fig. 3(a), two additional faint rows, marked by the arrows in Fig. 3(b), are also evident within each 4× period. The distance between the two adjacent faint rows was ~3.9 Å, and ~6.2 Å between a faint row and the adjacent brighter row. The corrugation of the brighter atomic rows along the [100] direction was typically about 1.5 Å when the sample was biased at 2.5 V. This corrugation, however, depended on the sample bias. It typically varied from 0.8 to 1.7 Å as the sample bias changed from 3.0 to 1.5 V, with the exact magnitude dependent on the tip. This bias dependence suggests a coupling between geometric and electronic effects in determining the contrast in the image.

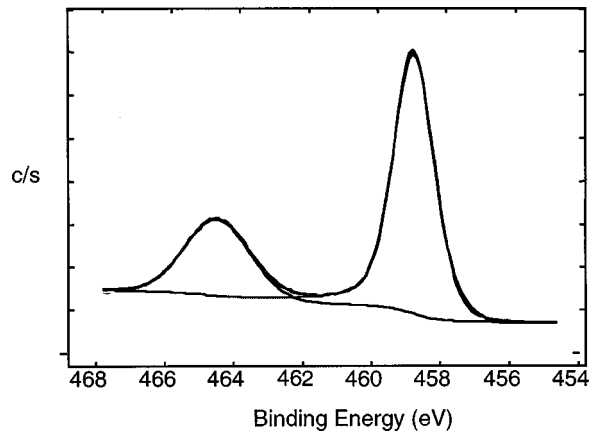

FIG. 4. XPS spectra of Ti $2p_{3/2}$ and Ti $2p_{1/2}$ core levels for an as-grown anatase (1×4) surface. The solid line is the experimental data and the dashed line is the fitted peak involving a single Gaussian-Lorentzian peak for Ti $2p_{3/2}$ and Ti $2p_{1/2}$, respectively. The excellent fit demonstrates the absence of Ti^{3+} on the $TiO_2(001)$-(1×4) surfaces.

In addition to the (4×1) reconstruction, local $3\times$ and $6\times$ reconstructions were also observed on this surface. Compared to the (1×4), these local reconstructions occurred much less frequently. Figure 3(c) is a STM image of a local $3\times$ reconstruction. It involves only two atomic rows with the spacing between them being ~12 Å. These results indicate that on $TiO_2(001)$ surfaces the separations between atomic rows can vary to some degree. Such a variability could be due either to defects related to stacking faults, or to ''added''-row structures such as those observed on rutile $TiO_2(110)$-(1×2) where variable row spacing is intrinsic.[15,16]

B. Electronic structures and stability of (1×4) reconstruction

In addition to surface morphology, atomic structures, and surface symmetry, the electronic structures of the anatase (001) surfaces were also investigated using XPS. Figure 4 is an XPS spectrum of the Ti core level for an as-grown (1×4) reconstructed anatase surface. Results show that both the Ti$2p_{3/2}$ and Ti$2p_{1/2}$ peaks can be fitted well by single peaks, indicating the absence of Ti^{3+} from the (1×4) reconstruction. To verify the stability of the (1×4) reconstruction, we annealed the surface in UHV and in oxygen plasma (oxygen partial pressure as high as 8×10^{-6} Torr) conditions with sample temperature up to 850 °C. STM and LEED showed that the (1×4) reconstruction remained unchanged. XPS of $TiO_2(001)$ showed no evidence of Ti^{3+} states after annealing in UHV at temperatures as high as 750 °C, a condition under which significant reduction is known to take place on rutile surfaces. Annealing at higher temperatures in UHV began to produce Ti^{3+} states observed by XPS. These results suggest that anatase $TiO_2(001)$-(1×4) is more stable toward reduction than rutile surfaces. Annealing the $TiO_2(001)$-(1×4) surface in oxygen plasma with oxygen partial pressure greater than 8×10^{-6} Torr often degraded the LEED pattern of the surface, resulting in either a weak (1×4) or sometimes a diffused (1×1) pattern. Prolonging the annealing time did not improve the quality of the LEED pattern.

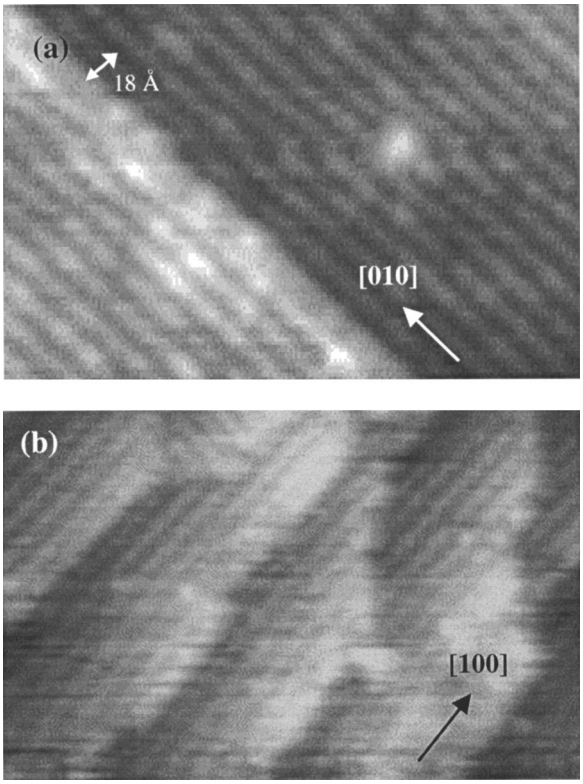

FIG. 5. (a) A STM image showing a double-height step running along the [010] direction. The separation between the two atomic rows from upper and lower terraces adjacent to the step edge is 18Å. The size of the image is 450×280 Å^2. (b) A STM image obtained on a vicinal surface, showing that the (1×4) domain dominates the surface. The normal of the surface had a 2° inclination toward the [010] direction.

C. Surface steps, domain boundaries, and domain population

In addition to the single-height steps shown in Fig. 3(a), double-height steps were also observed on $TiO_2(001)$-(1×4). Figure 5(a) is a STM image of a double-height step with its edge parallel to the atomic rows on the terraces. The lateral separation between the two adjacent atomic rows from the upper and lower terraces was ~18 Å, ~2 Å larger than the $4\times$ distance. In addition, the atomic row at the step edge on the upper terrace is typically broader than those on the regular terraces.

STM results showed that on $TiO_2(001)$-(1×4) the overall step direction dictated by the misorientation of the crystal profoundly affects the population of (1×4) and (4×1) domains. On nominally flat (001) surfaces where the step densities along [100] and [010] were nearly equal, the population of (1×4) and (4×1) domains were also approximately the same. For example, statistical analysis of Fig. 3(a) showed that the (1×4) domain occupied 48.3% of the total surface area while the (4×1) domain occupied 51.7%. The population distribution changed drastically on vicinal sur-

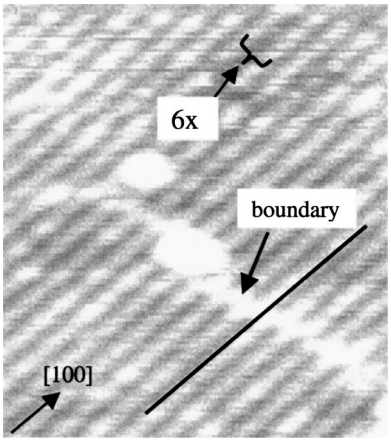

FIG. 6. A STM image showing two antiphase domains coexisting on the same terrace. The protrusions from one domain align with the depressions on the other domain, as demonstrated by the marked line. Near where the domain boundary ends, a local 6× reconstruction is also evident as demonstrated by the arrow.

faces. Figure 5(b) is a STM image obtained from a mineral TiO_2(001) surface that has a vicinal surface with 2° inclination toward the [100] direction. As a result, the majority of the steps had their edges along the [100] direction. Instead of the equal domain populations observed on the flat surface, the (1×4) domains, which had atomic rows running parallel to the [100] step edges, occupied nearly 92% of the total surface area. In contrast, the (4×1) domains occupied only 8% of the surface area, indicating that the steps strongly discriminated against the domains with atomic rows perpendicular to the step edges. This change in domain populations was also reflected by LEED measurements. LEED patterns taken on this vicinal surface showed that the (1×4) domains had a higher diffraction intensity than that of the (4×1) domains.

In addition to those orthogonal (1×4) and (4×1) domains, antiphase domains, nearly 180° out of phase with respect to each other, were also observed on the anatase (001) surface. In contrast to the (1×4) and the (4×1) domains, which were separated by single-height atomic steps, these antiphase domains coexisted on the same terrace. Figure 6 is a STM image of two antiphase domains. The right side of the image shows a domain boundary across which protrusions from one domain nearly align with depressions from the other domain. The domain boundary ends at the left side of the image, beyond which continuum atomic rows running along the [100] direction further confirmed that these two antiphase domains were on the same terrace. Near where the domain boundary ends at the left side of the image, a local 6× reconstruction, marked by an arrow, is also evident.

IV. DISCUSSION

The (1×4) reconstruction was observed previously by angle-resolved mass spectroscopy of recoiled ions and by LEED. This reconstruction was attributed to (103) and $(\bar{1}03)$ microfaceting by Herman *et al.*[10] and to missing oxygen rows by Hengerer *et al.*[11] Based on our investigation of the stability of the surface, the (1×4) reconstruction is not likely to be due to missing oxygen rows. This is because all anatase films we investigated were grown in an activated oxygen environment with the oxygen partial pressure as high as 2×10^{-5} Torr. Under these conditions, the (1×4) reconstruction was observed during growth by RHEED. If the (1×4) surface were reduced, continued growth on this surface would undoubtedly lead to films with a bulk stoichiometry considerably less than TiO_2, which is not the case. In addition, our XPS spectra of the (1×4) surface showed no evidence of Ti^{3+} at the surface. Furthermore, postgrowth annealing of the TiO_2(001)-(1×4) under reduction and oxidation conditions showed no substantial differences in STM, LEED, and XPS results. This experimental evidence suggests that the (1×4) reconstruction is fully oxidized and remains stable under these annealing conditions. Furthermore, since high-quality single-crystal anatase films were grown on these reconstructed surfaces, the (1×4) reconstruction is also not likely to be related to any nonanatase phases such as Ti_2O_3 or rutile TiO_2, but has the structural properties characteristic of anatase.

The (1×4) reconstruction is also not likely to be due to microfaceting toward the (103) and $(\bar{1}03)$ planes,[10] since this model is inconsistent with the high-resolution STM images shown in Fig. 3(b). It is known that under the positive sample bias condition STM preferentially images cation-derived states.[17] This was also verified by Diebold *et al.* on the rutile TiO_2(110) surface.[18] These authors found that on the rutile TiO_2(110) surfaces, although the oxygen atoms lie above the Ti atoms, it is the Ti-derived states that contribute to the STM images under the positive sample bias condition.[19] Since rutile and anatase have similar densities of states and hybridization of atomic orbitals in their conduction bands,[19] we expect that this finding on TiO_2 rutile[18] can also be applied to anatase surfaces. Consequently, according to the $(103)/(\bar{1}03)$ microfaceting model, one would expect to see no atomic rows within the (1×4) surface unit cell since there are no Ti-derived states. This is inconsistent with the high-resolution STM image shown in Fig. 3(b). The $(103)/(\bar{1}03)$ microfacet model also suggests pairs of Ti atoms at the tops of the ridges, but no such pairs could be resolved in high-resolution images.

Since the measured vertical separation between the bright and faint rows varied with sample bias, this apparent separation is a combination of geometric and electronic effects. It is worth noting that, if the bright and faint Ti rows had the same local electronic structures, their corrugations would change in the same way under different sample biases, resulting in a constant vertical separation between these rows. Since this contradicts the STM results, and because the 1.5 Å separation does not correspond to a characteristic distance between titanium atoms in anatase, the results indicate that the bright and faint rows are likely to have different local electronic structures.

Based on our STM, RHEED, LEED, and XPS results, it is quite clear that the (1×4) reconstruction cannot be adequately explained by previously proposed models.[10,11]

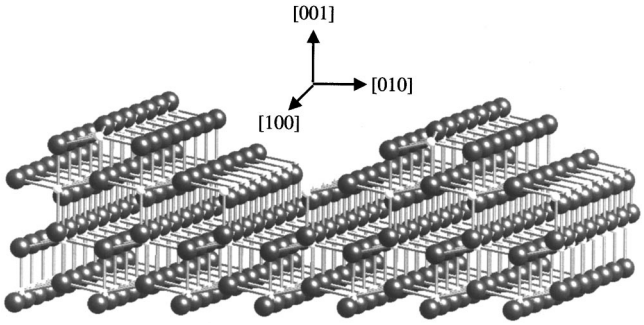

FIG. 7. A ball-and-stick model of the anatase $TiO_2(001)$-(1×4) reconstruction. Large and small balls represent oxygen and titanium atoms, respectively.

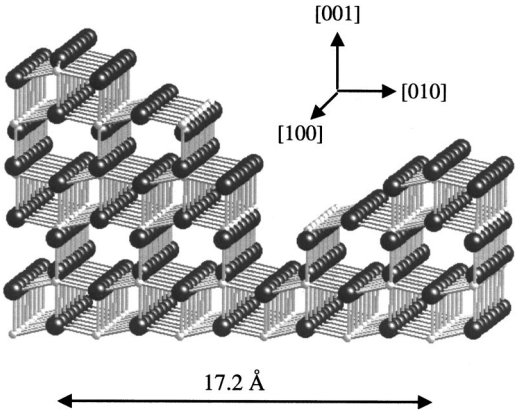

FIG. 8. A structural model of a double-height step based on the proposed (1×4) structure. The horizontal distance between the adjacent two atomic rows from the upper and lower terraces is 17.2 Å, consistent with the distance determined by STM.

Combining the experimental results obtained from this investigation, we propose the structural model shown in Fig. 7 for the (1×4) reconstruction. This model is based on the (1×1) surface structure, involving ''added'' and ''missing'' rows. All atoms in this model are derived from their bulk positions. Each surface unit cell consists of one added Ti-O row, two added oxygen rows, and one missing oxygen row. The resulting surface is stoichiometric and autocompensated in charge; thus not only is it energetically favorable, but it also contains no Ti^{3+} states, consistent with our XPS results. There is a similarity between this model and the $(103)/(\bar{1}03)$ microfaceting model.[10] Our model effectively creates microfacets toward the (014) and $(01\bar{4})$ planes. The major difference between these two models is that this one has two rows of Ti atoms within each unit cell, whereas the Ti atoms are missing in the $(103)/(\bar{1}03)$ microfaceting model. In addition, instead of being driven by surface faceting, the added-and-missing-row model allows the surfaces to form different reconstructions such as (1×3) and (1×6) by simply varying the spaces between the added and missing rows.

It is worth noting that within the framework of the proposed (1×4) model shown in Fig. 7 there are several ways to satisfy surface charge neutrality. One way is to completely remove the atomic oxygen row in the middle of the trough as shown in Fig. 7. This results in all the Ti atoms in the trough having fourfold coordination. Another way is to remove all the oxygen atoms on top of the added row instead of in the middle of the trough, resulting in all the Ti atoms on top of the added row being threefold coordinated; this is highly unrealistic. Finally, one can satisfy charge neutrality by removing half of the oxygen atoms from the trough and half from the top of the added row in each surface cell. This results in all the Ti atoms on top of the added rows being fourfold coordinated, and the Ti atoms in the middle of the trough being 50% fourfold coordinated and 50% fivefold coordinated. In this case, if all the missing oxygen atoms are structurally coherent, they yield a (2×4) reconstruction instead of the (1×4) reconstruction, thus contradicting our experimental results. However, if the missing oxygen atoms are not coherent along or between the rows, this structure produces a (1×4) reconstruction in the LEED pattern. We have recently conducted a STM investigation on the adsorption of formate on the anatase $TiO_2(001)$ surface.[20] The results showed that formate molecules preferentially adsorb on top of the added rows and form a local $2\times$ structure along these rows. While this local $2\times$ reconstruction should not be taken as an indication that the underlying TiO_2 surface must also have a $2\times$ periodicity, the preferential adsorption of formate on top of the added rows seems to suggest that the reduced coordination of Ti atoms on these rows, arguing against the complete removal of the oxygen row in the center of the trough. If the missing oxygen is distributed between the ''added'' rows and the troughs, then the preferential formate adsorption can be understood in terms of steric effects as well as other possible subtle differences between the ''added'' rows and troughs.

The added-and-missing-row model appears to reproduce the characteristic features of the STM images shown in Figs. 3(a) and 3(b); for example, bright rows 16 Å apart derived from the fivefold-coordinated Ti sites at the added Ti-O rows, and two faint rows about 4 Å apart within each unit cell resulting from tunneling into the fourfold-coordinated Ti sites. Since all the surface atoms from this reconstruction are derived from their bulk anatase positions, this reconstructed surface also serves as a good template for the growth of anatase films.

Based on this proposed model, we can also construct a double-height step that exhibits the characteristic distance features such as the 18 Å lateral separation and a broader atomic row at the step edge on the upper terrace shown in Fig. 5(a). Figure 8 is a ball-and-stick model of a double-height step structure. The resulting surface in this model is autocompensated. The separation between the two atomic rows from the upper and lower terraces adjacent to the step edge is 17.2 Å, consistent with the STM results shown in Fig. 5(a).

The driving force for the (1×4) reconstruction is unclear. The fact that the ideal anatase $TiO_2(001)$ surface reconstructs to a (1×4) structure although it is autocompensated is ratherunusual, but not unique. In fact, it was found after annealing in UHV at elevated temperatures that, although the surface stoichiometry remained unchanged, autocompensated

MnO(001) surfaces transformed from (1×1) to (2×2) and (6×6) reconstructions.[21]

In summary, we present a STM investigation on the surface reconstructions, steps, and domain population of anatase TiO_2(001). Combining STM, XPS, RHEED, and LEED results, the (1×4) surface reconstruction is explained in terms of added and missing rows at the surface. This model is also consistent with the observed step structures. In addition, the effects of surface steps on domain population were investigated. The results showed that single-height steps have a strong preference for domains with atomic rows parallel to the step edges. While the present work does not provide definite proof of the proposed model, it represents a good step forward toward understanding the properties of the anatase surface.

ACKNOWLEDGMENTS

This research was supported by PNNL Laboratory Directed R&D funds, and was performed in the Environmental Molecular Sciences Laboratory, a national scientific user facility sponsored by the Department of Energy's Office of Biological and Environmental Research. PNNL is a multiprogram national laboratory operated for the Department of Energy by Battelle Memorial Institute. E.I.A. acknowledges support from the Department of Energy BES Grant No. DE-FG-02-98ER14882. The authors thank David McCready for XRD characterizations of the anatase films, and acknowledge useful discussions with Dr. G. S. Herman and Dr. R. E. Tanner on anatase surface structures.

*Corresponding author. Email address: Yong.Liang@pnl.gov

[1] A. Fujishima and K. Honda, Nature (London) **238**, 37 (1972).
[2] J. T. Remillard, J. R. McBride, K. E. Nietering, A. R. Drews, and X. Zhang, J. Phys. Chem. B **104**, 4440 (2000).
[3] A. I. Kingon, J. P. Maris, and S. K. Steiffer, Nature (London) **406**, 1032 (2000).
[4] B. O'Regan and M. Gratzel, Nature (London) **353**, 737 (1991).
[5] S. Y. Huang, L. Kavan, I. Exnar, and M. Gratzel, J. Electrochem. Soc. **142**, L142 (1995).
[6] L. Forro, O. Chauvet, D. Emin, L. Zuppiroli, H. Berger, and F. Levy, J. Appl. Phys. **75**, 633 (1994).
[7] H. Tang, F. Levy, H. Berger, and P. E. Schmid, Phys. Rev. B **52**, 7771 (1995).
[8] M. Kamei and T. Mitsuhashi, Surf. Sci. **463**, L609 (2000).
[9] G. Durinck, H. Poelman, P. Clauws, L. Fiermans, J. Vennik, and G. Dalmai, Solid State Commun. **80**, 579 (1991).
[10] G. S. Herman, M. R. Sievers, and Y. Gao, Phys. Rev. Lett. **84**, 3354 (2000).
[11] R. Hengerer, B. Bolliger, M. Erbudak, and M. Gratzel, Surf. Sci. **460**, 162 (2000).
[12] S. A. Chambers, Y. Gao, S. Thevuthsan, Y. Liang, N. R. Shivaparan, and R. T. Smith, J. Vac. Sci. Technol. A **14**, 1387 (1996).
[13] S. Gan, Y. Liang, and D. R. Baer, Surf. Sci. **459**, L498 (2000).
[14] Y. W. Mo, B. S. Swartzentruber, R. Kariotis, M. B. Webb, and M. G. Lagally, Phys. Rev. Lett. **63**, 2393 (1989).
[15] C. L. Pang, S. A. Haycock, H. Raza, P. W. Murray, and G. Thornton, Phys. Rev. B **58**, 1586 (2000).
[16] H. Onishi and Y. Iwasawa, Phys. Rev. Lett. **76**, 791 (1996).
[17] R. Wiesendanger, *Scanning Probe Microscopy and Spectroscopy—Methods and Applications* (Cambridge University Press, Cambridge, England, 1994).
[18] U. Diebold, J. F. Anderson, K. Ng, and D. Vanderbilt, Phys. Rev. Lett. **77**, 1322 (1996).
[19] S. Mo and W. Y. Ching, Phys. Rev. B **51**, 13 023 (1995).
[20] R. E. Tanner *et al.* (unpublished).
[21] R. J. Lad and V. E. Henrich, Phys. Rev. B **38**, 10 860 (1988).